1949-08-01

Magnus effect on a body of revolution at various angles of attack

Stefan, Karl Henry

St. Paul, Minnesota; University of Minnesota

MAGNUS EFFECT ON A BODY OF

REVOLUTION AT VARIOUS ANGLES OF ATTACK

by

Karl H. Stefan

Lt. Commander, U. S. Navy

Department of Aeronautical Engineering

University of Minnesota

Minneapolis, Minnesota

August 1, 1949

A Thesis Submitted to the Faculty of the Graduate School

in Partial Fulfillment of the Requirements for the

Degree of Master of Science

TABLE OF CONTENTS

LIST OF FIGURES

SUMMARY

This paper investigates the Magnus force as it occurs on a rotating cylindrical body with a conical nose in flight at high subsonic velocities and at small angles of attack.

The comparison of experimental results with a simplified theoretical analysis indicates that empirical data is necessary in order to evaluate the Magnus force. An empirical curve suitable for the model tested is presented.

The position of the center of pressure for the Magnus force is also investigated, and empirical data for the location of this point is presented. The position of the center of pressure was found to be a function of rotational velocity and angle of attack.

Experimental results compared favorably with the results of previous investigators where test conditions were duplicated. However, no previous work was available for the tests at small angles of attack.

LIST OF SYMBOLS

U_s Free stream velocity

U_o Component of U_s perpendicular to axis of model

U Local tangential velocity at surface of cylinder due only to transverse airflow

V Peripherial velocity of the cylinder surface

V_v Vortex velocity at radius under consideration

V_1 Total local velocity

M Mach Number

ω Angular velocity

p absolute pressure at any point

p_o Stagnation pressure

p_s Absolute static pressure in the free stream

ρ Density

L Magnus Effect or Magnus force

Γ Circulation

C_L Magnus Effect coefficient based on U_s

C_{Lo} Magnus Effect coefficient based on U_o

C_L Magnus Effect coefficient for infinite aspect ratio

q_s Dynamic pressure based on U_s

q_o Dynamic pressure based on U_o

α Angle of Attack, defined as angle between freestream velocity and the axis of the cylinder

θ Angular position on cylinder measured from the upstream point of the cylinder

LIST OF SYMBOLS (con't.)

r Radius

ℓ Length

S Area of model profile ($dS = 2r \times d\ell$)

R_n Reynolds number

MAGNUS EFFECT ON A BODY OF REVOLUTION AT VARIOUS ANGLES OF ATTACK

I. INTRODUCTION

When a body of revolution, such as a cylinder, is rotated about its axis of revolution and is placed in an airstream perpendicular to the axis, a force is generated which is perpendicular to the airstream direction and to the spin axis. This force is termed "Magnus Effect" after the man who first demonstrated its existence in 1852 (1).

The development of the circulation theory of lift by Prandtl (2) broadened the theoretical aspect of the Magnus Effect, and it has been accordingly rather closely investigated in the case of the spinning cylinders with comparatively low speed airflow perpendicular to the spin axis by Betz, Reid, and Busemann (3,4). These investigations showed that remarkably high lift coefficients were obtainable although at the expense of considerable drag. The fact that the Magnus Effect can be of considerable magnitude has prompted several commercial ventures such as the Flettner Rotor Ship and the Madaras Rotor Power Plant.

Spinning projectiles are subject to this force whenever there is any transverse component of flow over the body. Since the magnitude of this force has been considered small in comparison to gyroscopic forces of the body, it has not been investigated thoroughly in discussions of projectile stability

and trajectory. However, in certain recently developed missiles the question has arisen of the importance of this force in the development of instability.

It is the purpose of this paper to investigate the magnitude and position of this force vector as it occurs on a basic geometric shape travelling at subsonic speeds at a small angle of attack. The model configuration to be tested is that of a cylinder with conical nose.

Rotation of a body in a transverse airflow also has an effect on drag since rotation has a profound effect upon the character of separation of flow from the surface. The effect on drag is beyond the scope of this paper, but in any overall analysis of the aerodynamic effect of rotation, it would have to be considered.

Appreciation is expressed to Professor John D. Akerman, Adviser and Head of the Aeronautical Engineering Department, University of Minnesota, under whose direction this thesis was written, and to staff members of the Rosemount Research Center who assisted in the wind tunnel experimental work.

II. METHODS

A. Theoretical

An exact theoretical computation of the "Magnus Effect" force in the case of a body of revolution at an angle of attack becomes complicated, if not impossible, because of

the number of variables and unknowns involved and the complex relationships between them present difficult mathematical problems. It is, therefore, necessary to rely upon theory as only a rough guide to the magnitude of forces involved and to rely on experimental data for qualitative information.

Accordingly, in this paper a theoretical discussion of the various factors which affect this force will be given, and then the experimental results of the force as found on the model will be discussed. It will be seen that the experimental equipment and procedure are adaptable to practically any model configuration and test conditions.

The body to be discussed in the theoretical analysis is a cylinder with conical nose set at a small angle of attack, spinning about its axis and travelling at subsonic velocities. (Figure I.) The problem is to determine the magnitude and location of the Magnus Effect force acting on the body.

The obvious theoretical approach is to determine the pressure distribution over the surface of the body, and then to integrate the components of pressure acting in the direction normal to the free-stream and the cylinder axis. (Figure II.)

If the component of free-stream air flow perpendicular to the cylinder axis is considered to be the only velocity component affecting the Magnus force, the problem may then be approached as the analysis of two dimensional flow of air over a long rotating cylinder with its axis normal to the

airflow. (Figure II.)

An analogous flow field is developed from purely theoretical considerations for an incompressible, non-viscous fluid by Prandtl (2). This is accomplished by the superposition of a vortex flow and the flow about a cylinder with the final velocity at any point being the sum of the two superposed velocities. In this case, the Magnus force may be computed as follows: (In the references, the force is called "lift", but it will be referred to here as "Magnus" force.)

From perfect fluid theory for a non-rotating cylinder:

$$U = 2\, U_o \sin\theta$$

then $V = 2\, U_o \sin\theta + V_v$

At any point, by Bernoulli's Equation:

$$p = \frac{1}{2}\rho\, (V^2 - U_o^2)$$

Total Magnus Effect force per unit span becomes:

$$L = \oint \Delta p \sin\theta\, r\, d\theta = \oint \frac{1}{2}\rho (V^2 - U_o^2) r \sin\theta\, d\theta$$

$$= \oint \frac{1}{2}\rho\, r\, V^2 \sin\theta\, d\theta$$

$$= \oint \frac{r\rho}{2}\, (4\, U_o^2 \sin^2\theta + 4\, U_o V_v \sin\theta + V_v^2) \sin\theta\, d\theta$$

$$= \oint 2r\, \rho\, U_o V_v \sin^2\theta\, d\theta = 2r\rho U_o V_v \left[\frac{1}{2}\theta + \frac{1}{4} \sin 2\theta\right]_0^{2\pi}$$

$$= 4\pi r\, \rho\, U_o V_v = \rho\, U_o\, (2\pi r\, V_v)$$

Let $\Gamma = \oint V_v\, r\, d\theta = 2\pi r\, V_v$ (circulation)

$$L = \rho\, U_o\, \Gamma$$

Some adjustment of this result is required in order to

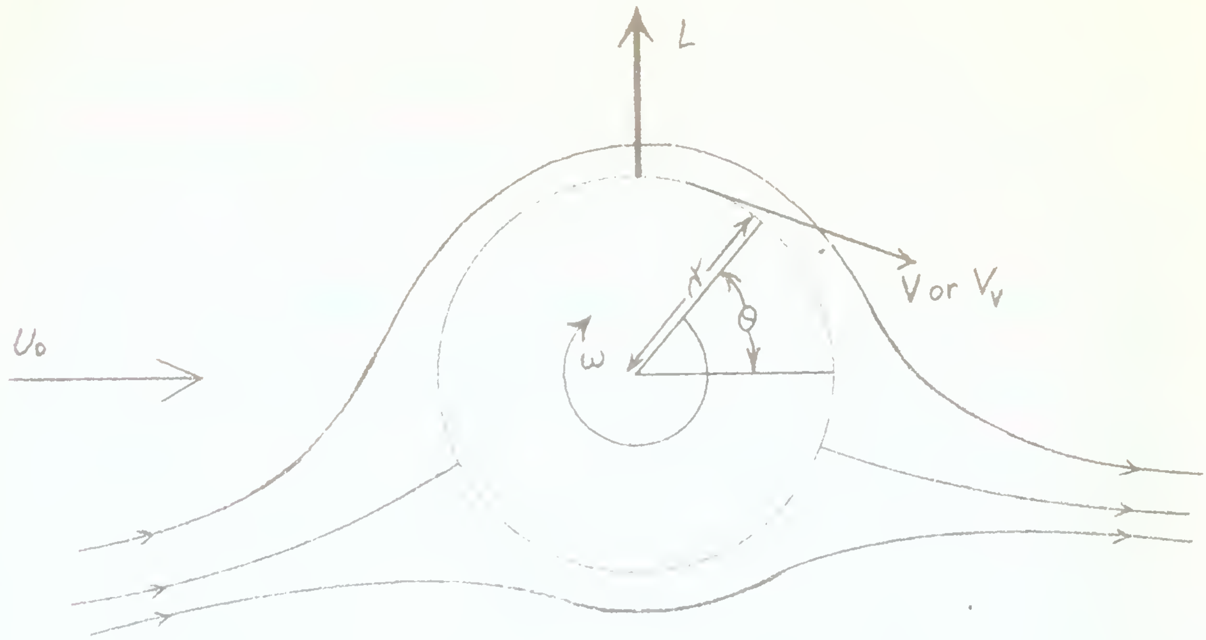

FIG. II - INFINITE CYLINDER IN TRANSVERSE AIRSTREAM

apply it to flow about a solid body. A cylinder in rotation sets up a circulatory flow about itself due to viscosity effects in the fluid and friction between the surface and the fluid. This flow, however, cannot be treated in the same manner as the fictitious vortex flow, because it is dependent on boundary layer velocity and pressure gradients. The process by which circulation is developed about a cylinder is discussed by Prandtl (2) and Goldstein (3) with the conclusion that the circulation induced by a cylinder is just half that of the equivalent surface in vortex motion. That is, for a cylinder, $\Gamma = \pi r V$. With Γ so determined, the flow pattern over a rotating cylinder is the same as with vortex flow at the same value of Γ. From Goldstein (3) and as seen on Figure III, when Γ reaches a value of $4 \pi r U_o$, the leading and trailing stagnation points coincide. With a cylinder this condition gives the equation:

$$\pi r V = 4 \pi r U_o$$

or,

$$V = 4 U_o$$

For a cylinder, this represents the condition for maximum Magnus force on the cylinder. This conclusion is reached by Goldstein (3). Any further increase in V carries fluid completely around the cylinder eliminating interaction of the cylinder surface and the free stream air flow. Thus, no further vortex action which will induce increased

FIG. III - THEORETICAL FLOW ABOUT ROTATING CYLINDER

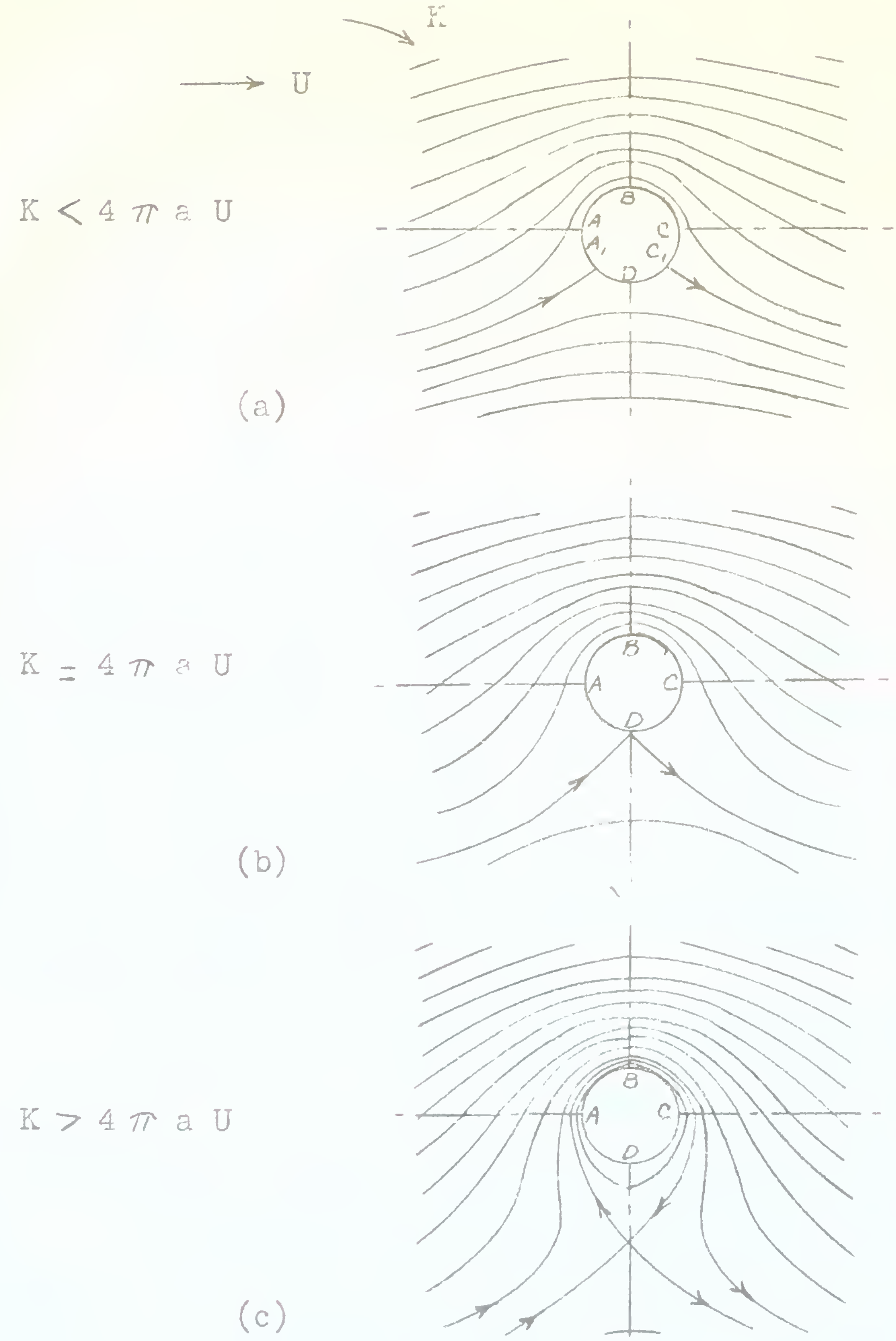

From: Goldstein, S., <u>Fluid Dynamics</u>, Vol. 1, p. 33

circulation occurs in the boundary layer.

It is convenient to express Magnus force in coefficient form. For the present, this coefficient will be given in terms of U_o:

$$C_{L_o} = \frac{L}{qS} = \frac{\rho U_o \pi r V}{\frac{1}{2} \rho U_o^2 (2r)} = \pi \frac{V}{U_o}$$

Since L_{max} occurs when $V = 4\,U_o$, then:

$$C_{L_{omax}} = 4 = 12.6$$

Experimental data on rotating cylinders as given by Goldstein (3) is presented in Figure IV. This shows that even with end effects eliminated by using end disks, the experimental values of C_{L_o} are somewhat less than the theoretical values as given above, and a maximum C_{L_o} of 12.6 is not reached. The reason for this discrepancy probably lies in the fact that separation of flow effects and viscosity are not considered in the theory.

Calculation of separation effects would involve determination of the area affected by separation and the pressure in this area. No exact solution for this problem exists.

In the case of a cylinder of finite length, a loss of Magnus force occurs due to spillage of pressure over the ends. The loss here may be investigated in the same manner as in airfoil theory, which is presented in detail by Prandtl (1) and Millikan (5). Briefly, the tip vortices induce a downwash velocity which changes the angle of incidence of the transverse velocity on the cylinder, and hence changes the direction of the Magnus force vector. When the Magnus force coefficients

FIG. IV - LIFT ON ROTATING CYLINDERS

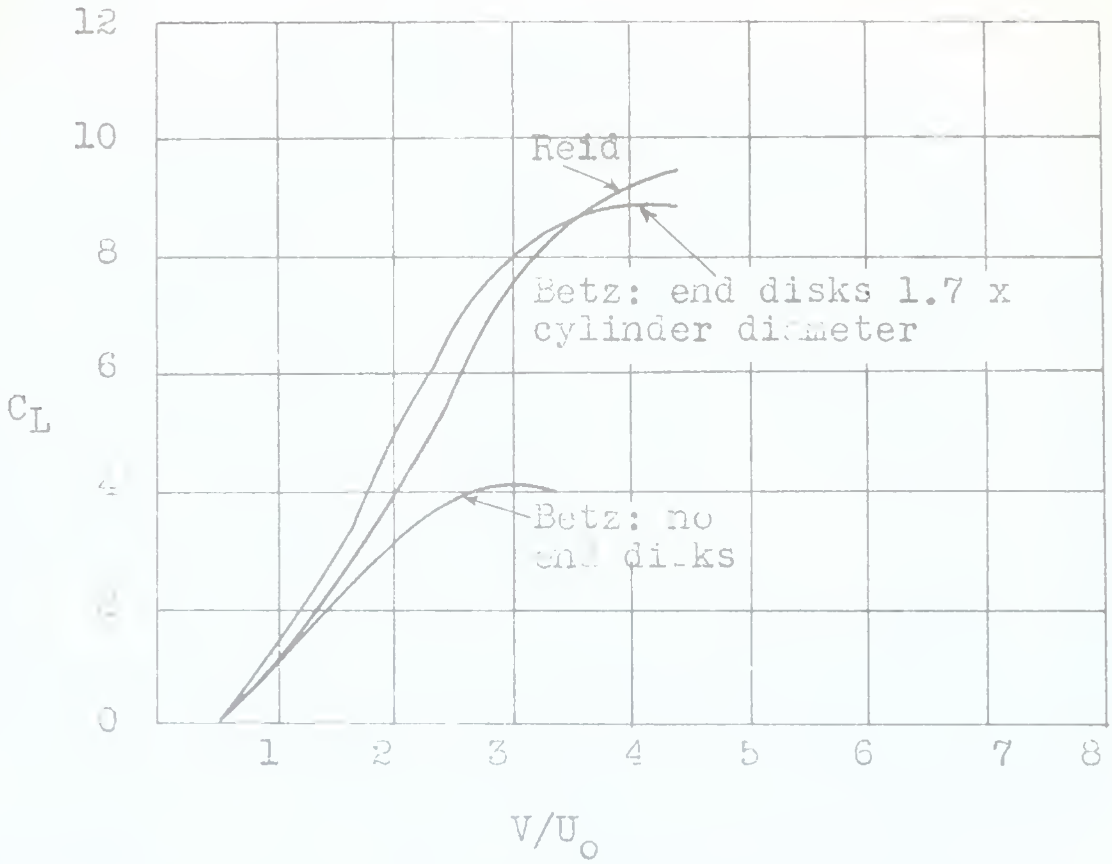

Reid: Aspect ratio 13.3; Reynolds number 3.9×10^4 to 1.16×10^5; no end disks.

Betz: Aspect ratio 4.7; Reynolds number $5.$[illegible]$\times 10^4$

From: Goldstein, S., "Fluid Dynamics", p. 546.

are small, corrections may be made by taking the desired component of the shifted vector. That is:

$$C_{L_c} = C_{L_{c\infty}} \cos \Delta\alpha$$

From Millikan (5), a suitable formula for $\Delta\alpha$ is obtained which gives good results for coefficients less than 1.5:

$$\Delta\alpha = \frac{C_L}{\pi\, AR} \quad (2.15)$$

This equation is derived with the assumption of small downwash velocities. With larger Magnus force coefficients, this assumption is no longer valid. Figure IV illustrates that after a certain point further increases in circulation produce a decrease in Magnus force. An explanation of this effect is given in Figure V.

Thus far this discussion has assumed the airstream direction to be perpendicular to the cylinder axis, whereas the object of this paper is to consider a model with its axis at a small angle of attack.

By assuming the only flow acting to be that component perpendicular to the axis, some error is introduced. The extent of this error can only be determined by experiment, but it is probably small as indicated by the following remarks.

First, the axial component of flow produces only axially symmetric pressure distributions which would have no effect on the non-symmetric force which is to be considered.

FIG. V - DOWNWASH EFFECT ON MAGNUS FORCE

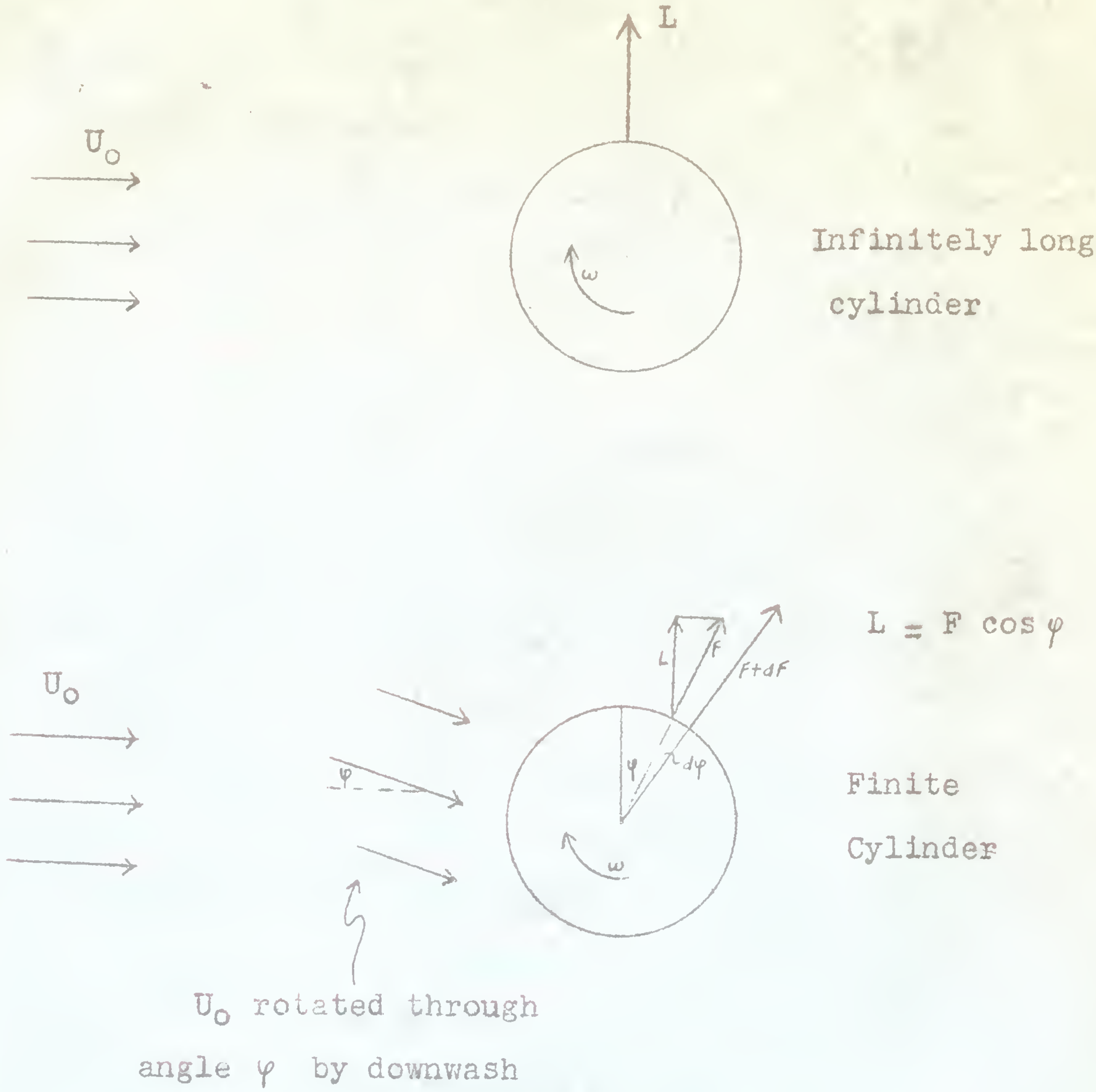

An increase in circulation increases F by dF and φ by $d\varphi$

Then,

$$L + dL = (F + dF)\cos(\varphi + d\varphi)$$

Since $\cos(\varphi + d\varphi)$ is a decreasing function which decreases to zero and F+dF must remain finite, a point will be reached where

$$(F + dF)\cos(\varphi + d\varphi) < F\cos\varphi$$

so that $(L + dL) < L$, or dL is negative.

Compressibility effects need not be considered, for the velocity component perpendicular to the axis will be sufficiently small so that it may be assumed incompressible. With a maximum free stream Mach Number of one, and a maximum angle of attack of 10°, the cross-flow has a maximum Mach Number of about one-tenth. With this cross-flow Mach Number, the maximum error introduced by use of Bernoulli's equation, instead of a compressible equation, is found to be 1.4%. For the same maximum conditions the error introduced by assuming incompressibility in developing the flow field is found to be less than 1%. This was computed by formulae developed by Sauer (6).

The center of pressure for the Magnus force can be estimated by assuming a pressure distribution in accordance with the foregoing discussion and calculating the position of the resultant as shown in Figure VI. For the particular configuration used in this investigation, the estimated losses are equal for each end; therefore, the center of pressure should be in the same place as it would be with no end effects.

It is necessary to develop a coefficient based on free stream velocities (U_o) and a non-dimensional parameter for plotting and comparing various experimental values and theoretical values. The coefficient is:

$$C_L = L/qS \quad \text{where} \quad q = \tfrac{1}{2} \rho U_o^2$$

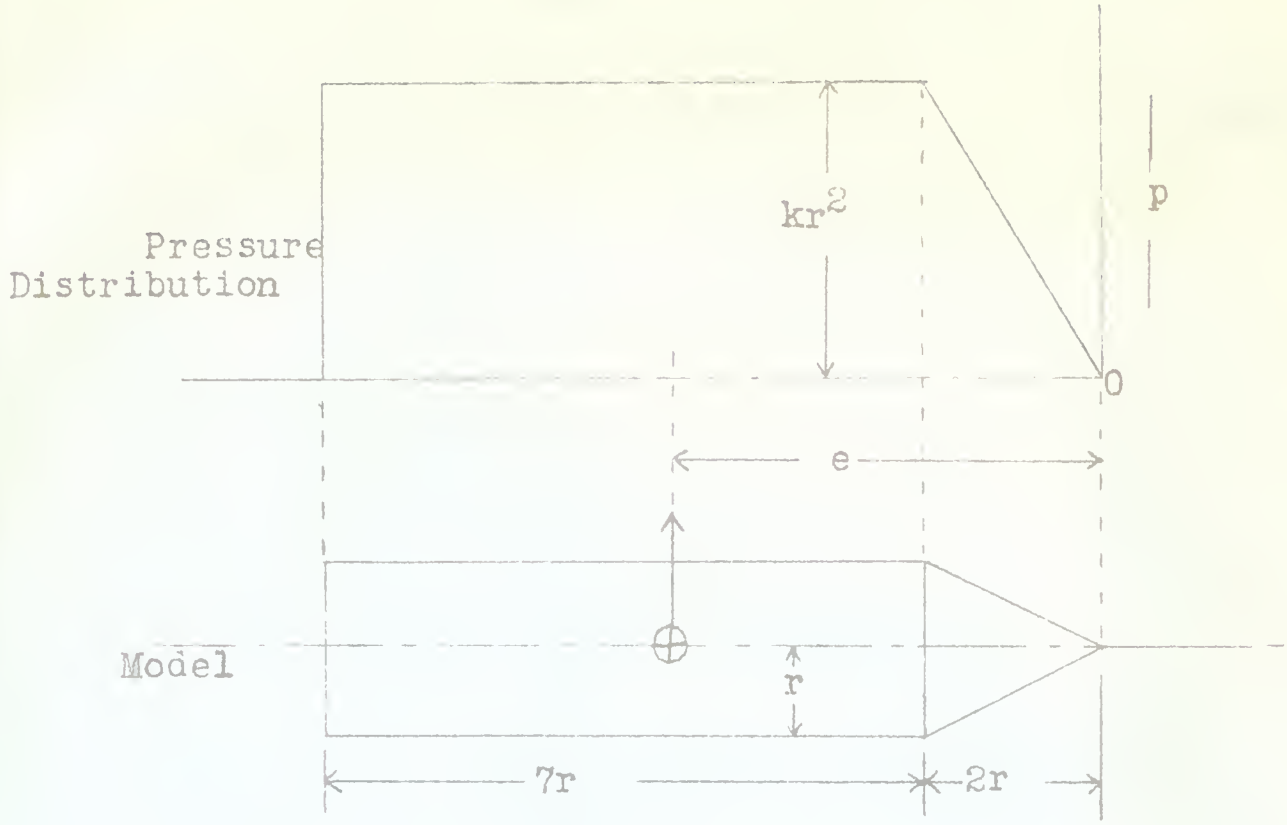

It is assumed the end effects balance each other so that the center of pressure is in the same position with or without end effects.

Taking area moments of the pressure distribution about the zero position:

$$\Sigma M = (kr^2)(r)(4/3\ r) + (kr^2)(7r)(5\tfrac{1}{2}\ r) = 39.833\ kr^4$$

then,

$$e = \Sigma M/\Sigma A = 39.833kr^4 / 8\ kr^3 = 4.98\ r$$

FIG. VI - CALCULATION FOR CENTER OF PRESSURE LOCATION

To find a suitable non-dimensional parameter, the following procedure is used:

$$C_L = L/qS$$

$$L = \rho \, U_o \, \Gamma$$

$$\Gamma = \pi \, r \, V$$

$$U_o = U_s \sin \alpha$$

$$q = \tfrac{1}{2} \rho \, U_s^{\,2}$$

$$S = 2\,r \times 1 = 2r$$

$$C_L = \frac{\rho \, U_s \sin \alpha \, \pi \, r \, V}{\frac{1}{2} \rho \, U_s^{\,2} \; 2\,r} = \pi \left(V/U_s \right) \sin \alpha$$

From the above it is seen that the factor $\left(V/U_s \right) \sin \alpha$ is a suitable parameter for use in determination of C_L.

For comparison of the data of this test with the two dimensional experiments of previous investigators, the coefficient C_{L_o} (already defined) will be used. By a mathematical derivation similar to the one above, it is seen that

$$C_{L_o} = L/q_o S = \pi \, V/U_o$$

so that the factor V/U_o is suitable parameter for the two dimensional comparisons.

B. Experimental

1. Equipment

Tests were conducted in the Transonic Windtunnel at the Rosemount Research Center of the University of Minnesota. The windtunnel, as shown in Figure VII, is an induced flow tunnel in which air ejectors downstream of the test section

FIG. VII - TRANSONIC WINDTUNNEL

create a low pressure area which induces flow through the test section from the atmosphere. The test section is square, 16" x 16", and subsonic speeds up to Mach Number .85 are obtainable with a model of the size tested.

The model, a brass cylinder with a conical nose, and accessories are shown with dimensions in Figures VIII, (a) and (b). The surface of the model was smooth machined and polished with fine emery cloth. The model was hollow and fitted with two sets of ball bearings near the forward end, and these bearings were mounted on the sting. The sting in turn was extended rearwards from the model to rigid supporting arms which were bolted to the test section windows. An air motor was attached to the rear end of the assembly, and it provided motive power for spinning the cylinder. Torque was transmitted from the motor to the nose of the cylinder by means of a 1/16" diameter shaft which passed through a 1/8" diameter hole extending along the axis of the sting. Flat surfaces were machined at three stations on the sting as shown in Figure VIII, and strain gages were mounted on these surfaces. Electrical leads from the gages went through the supporting arms and out of the tunnel to the external circuit. Strain gage circuits were Wheatstone bridge circuits, and strain values were read as shown by deflections of the galvanometer. A separate circuit was used for each pair of gages. A diagram of the circuit is given in Figure IX.

The model and accessory apparatus are shown (a) in sections,

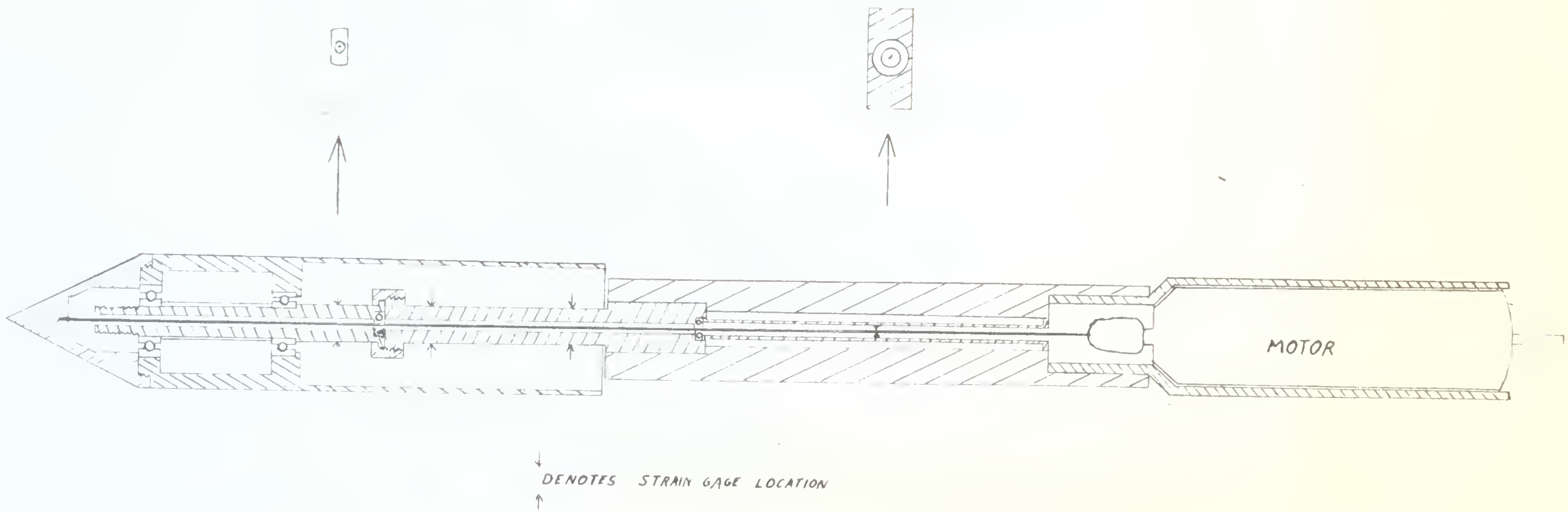

FIG VIII (a) MODEL CONFIGURATION

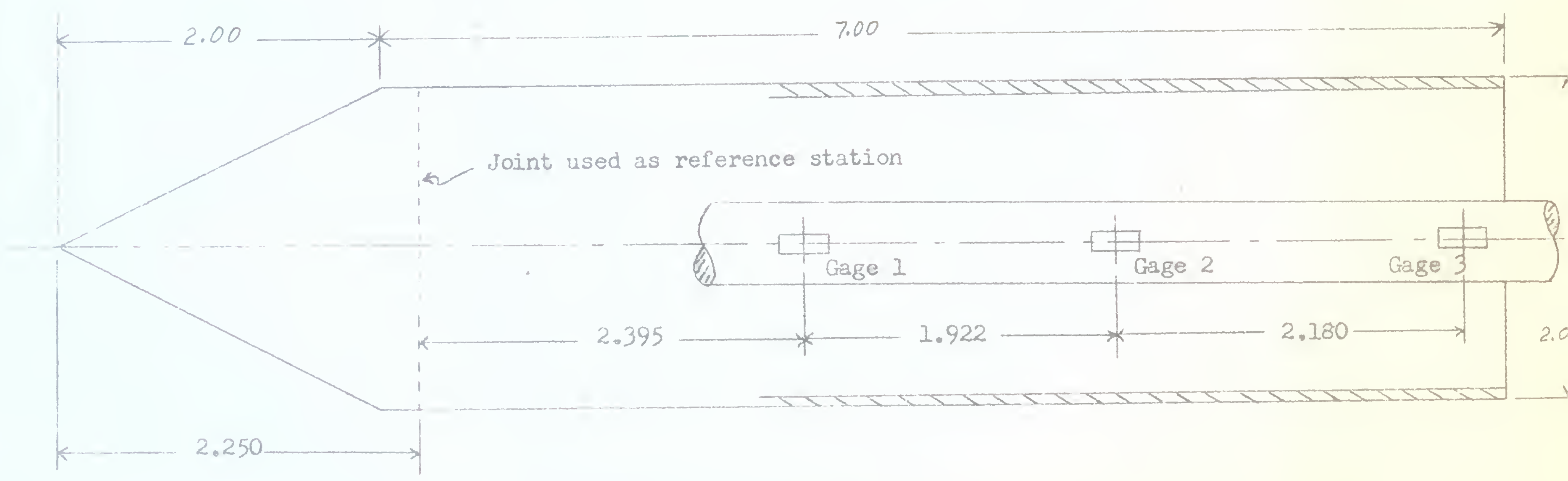

FIG. VIII(b) LOCATION OF STRAIN GAGES ON MODEL

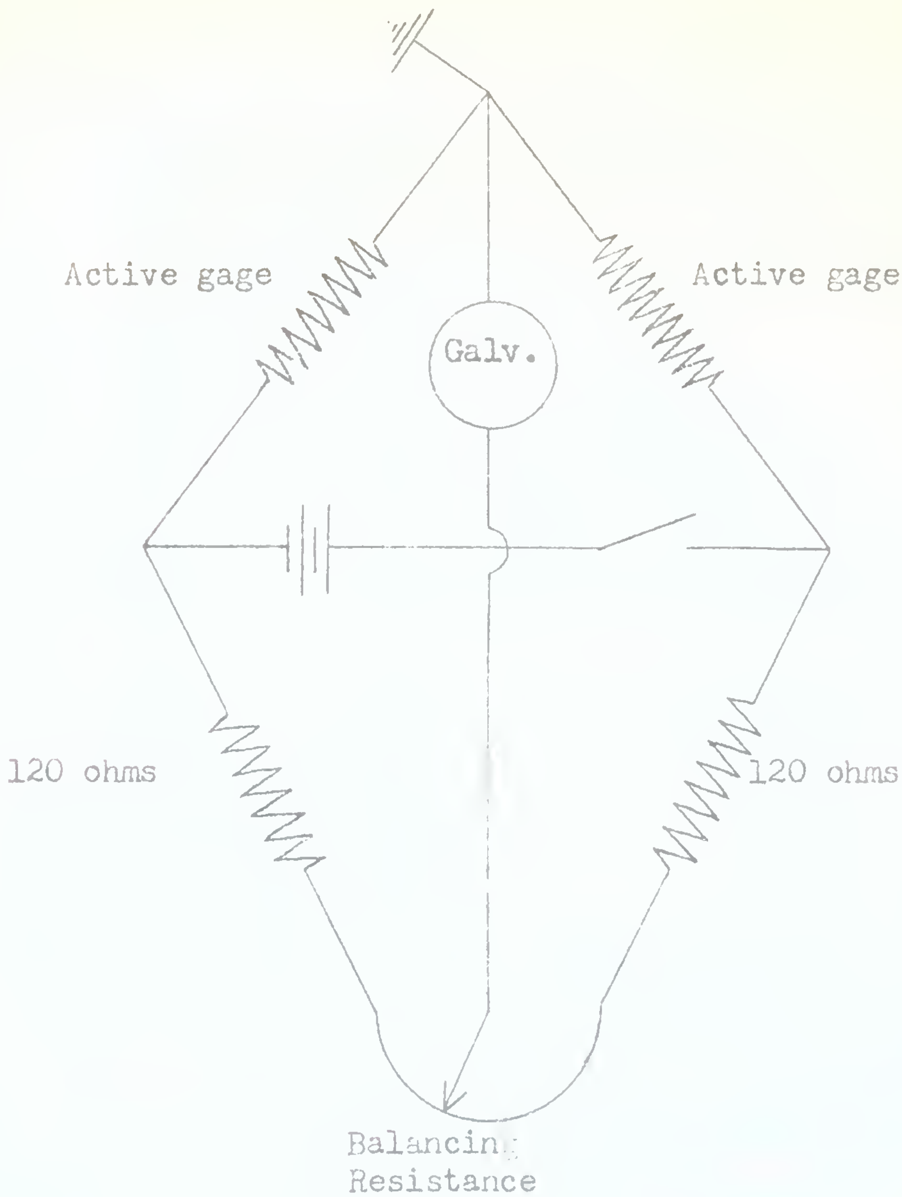

FIG. IX - STRAIN GAGE CIRCUIT DIAGRAM

(b) assembled, and (c) mounted in the windtunnel in the photographs of Figures I to XIV. The windows to which the model supporting arms were attached could be rotated so that the angle of attack of the model was changed in a vertical plane by rotating the windows. Compressed air was supplied to the air motor by a hose connection at the rear end of the motor, and the motor speed was regulated by a valve in the compressed air line outside the tunnel.

The rate of spin was read by a stroboscope operated by an observer at a window. A painted spiral line on the model provided the reference for smooth stroboscopic observation.

Operating limits of the apparatus were as follows:

Rate of spin - 0 to 20,000 rpm

Angle of attack - 0° to 15°

Windtunnel free air stream - Mach No. 0 to .75

A second arrangement for mounting the model was made so that the model projected into the tunnel with its axis perpendicular to the air stream. This arrangement is shown in the photograph of Figure XV. The clearance between the base of the model and the window from which it projected was 1/17 inch. The strain gages were oriented so as to measure forces acting in the direction perpendicularly to the air stream and to the model axis.

2. Test Procedure

The strain gage galvanometers were calibrated for

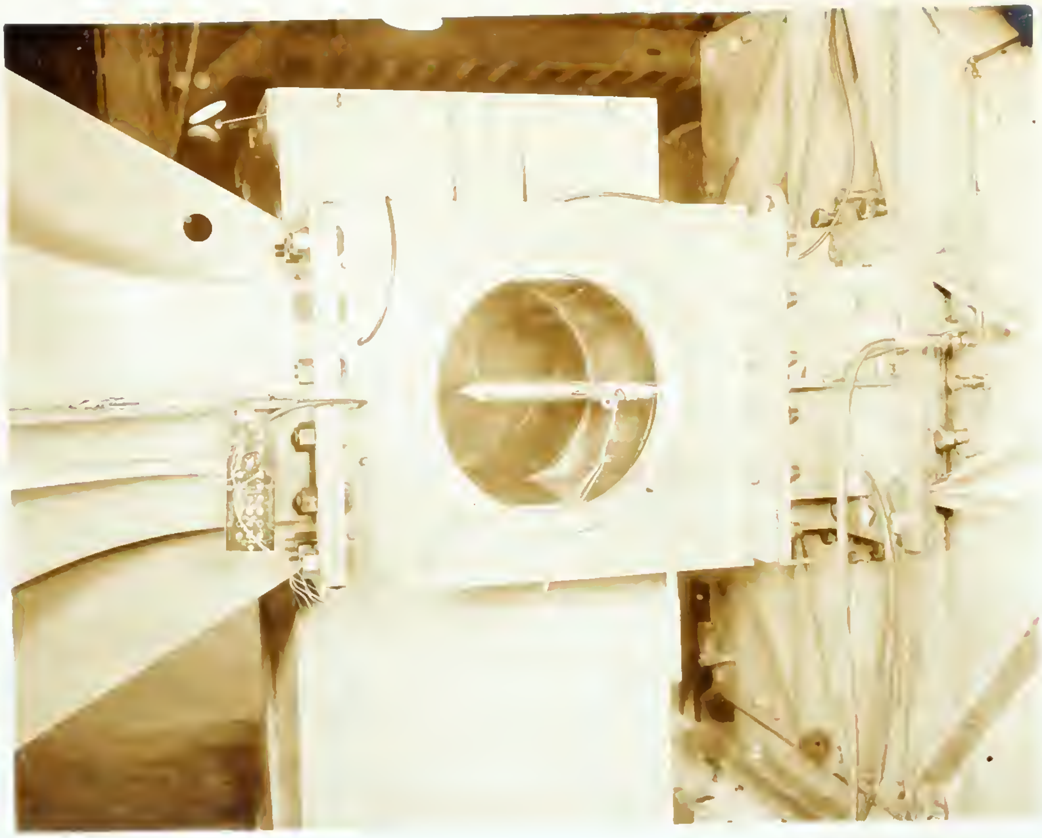

FIG. V - VIEW OF TEST SECTION WITH MODEL INSTALLED

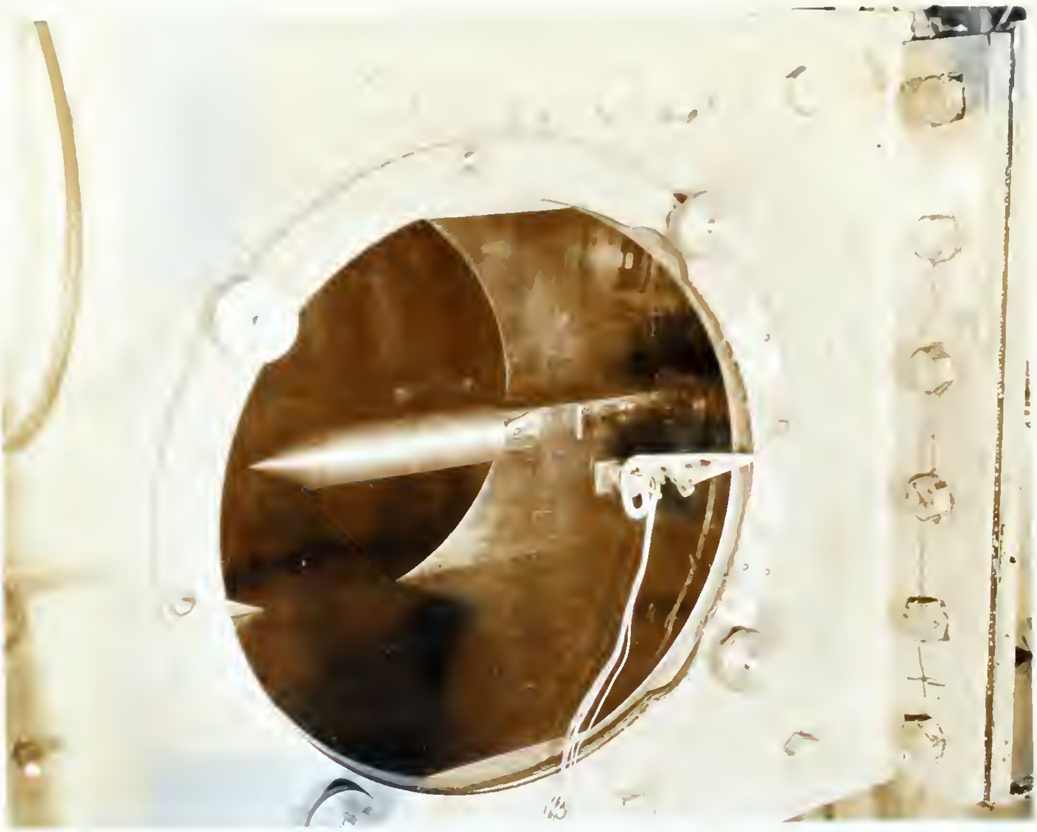

FIG. XI - SIDE VIEW OF INSTALLED MODEL

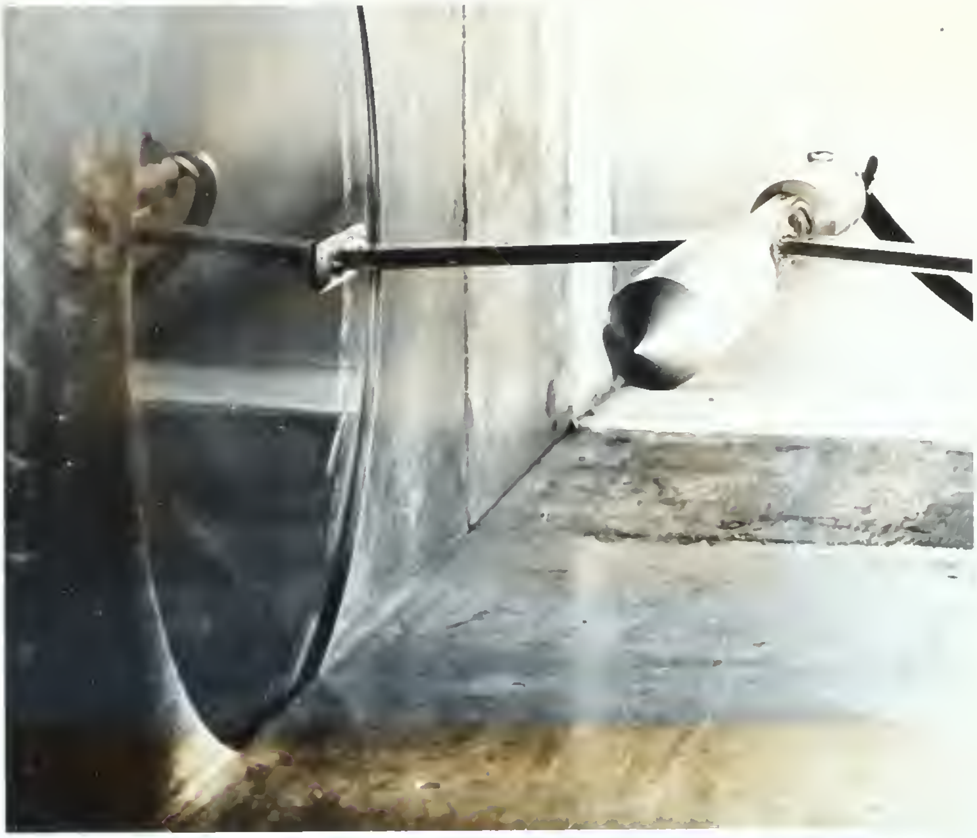

FIG. XII - FRONT VIEW OF INSTALLED MODEL

FIG. XIII - VIEW SHOWING SUPPORTING ARMS

FIG. XIV - MODEL SHOWN IN SECTIONS

FIG. XV - TWO VIEWS OF MODEL MOUNTED PERPENDICULAR TO TUNNEL WALL

conversion of readings to moments (in foot-pounds). This was accomplished by applying known forces to the model and reading corresponding galvanometer deflections.

Windtunnel velocity calibration was taken from previous calibration data of the Rosemount Research Center.

The model was mounted in the tunnel, set at an angle of attack, and a rate of spin was established, and then the windtunnel was started. Readings were taken from the galvanometers at four windtunnel airspeeds. The tunnel then was stopped, the angle of attack and rate of spin readjusted, and the tunnel was again started. This process was repeated through the various conditions to give all the necessary data.

To reduce the data to the form desired, the galvanometer readings were converted to moments, and these moments used to calculate the force acting and its center of pressure.

In order to separate out forces other than the Magnus force, it was necessary to obtain the normal force which was due only to misalignment of the model and not dependent on rotation. Therefore, force readings were taken at zero spin at the various angles of attack. Also, since the Magnus force gives a small deflection to the model, a normal force develops because of this deflection. Therefore, data was obtained giving normal force versus angle of attack. For each Magnus force measured, a corresponding deflection was obtained by

applying an equivalent force and measuring the model deflection. With this deflection, a normal force was obtained which was subtracted from the measured Magnus force to give the true Magnus force.

The Magnus force was then converted to coefficient form, and the data plotted on graphs.

With the second arrangement in which the model was perpendicular to the air stream, the tests were run at free stream velocities corresponding to the cross-flow velocity obtained in the first tests and at the corresponding rotation speeds. Recording and reduction of data was accomplished in the same manner as in the first experiment with the exception that the correction for model deflection was not necessary.

3. Discussion of Results

Figure XVI is a graphical presentation of Magnus force as it exists at various peripheral velocities, free stream velocities and angles of attack. This figure was prepared from data in the following ranges: Mach Number of .45 to .75; peripheral velocities of 0 to 170 ft./sec.; angles of attack of 0° to 15°; Reynold's Number (free stream) of 2.9×10^6 to 4.8×10^6.

In order to examine the relationship between this data and the theoretical factors discussed previously, it is convenient to present the Magnus force as a function of the cross flow velocities as shown on Figure XVII. In this figure it

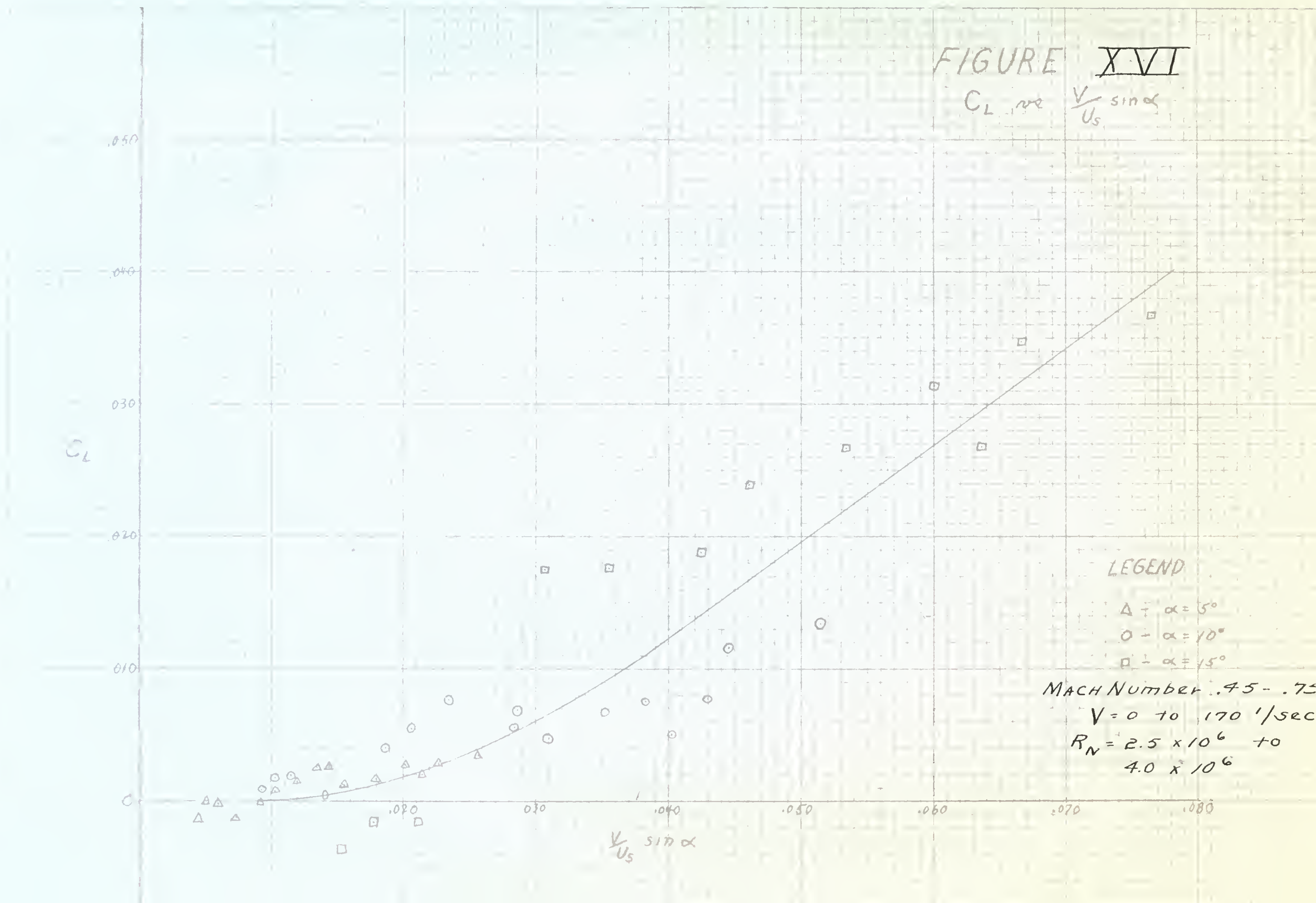
FIGURE XVI
C_L vs $\frac{V}{U_s}\sin\alpha$
.050
.040
.030
.020
.010
0
C_L
.020
.030
.040
.050
.060
.070
.080
$\frac{V}{U_s}\sin\alpha$
LEGEND
△ - α = 5°
○ - α = 10°
□ - α = 15°
MACH Number .45 - .75
V = 0 to 170 '/sec
R_N = 2.5 x 10^6 to
4.0 x 10^6

FIGURE XVII

C_{L_0} vs V/U_0 at various α

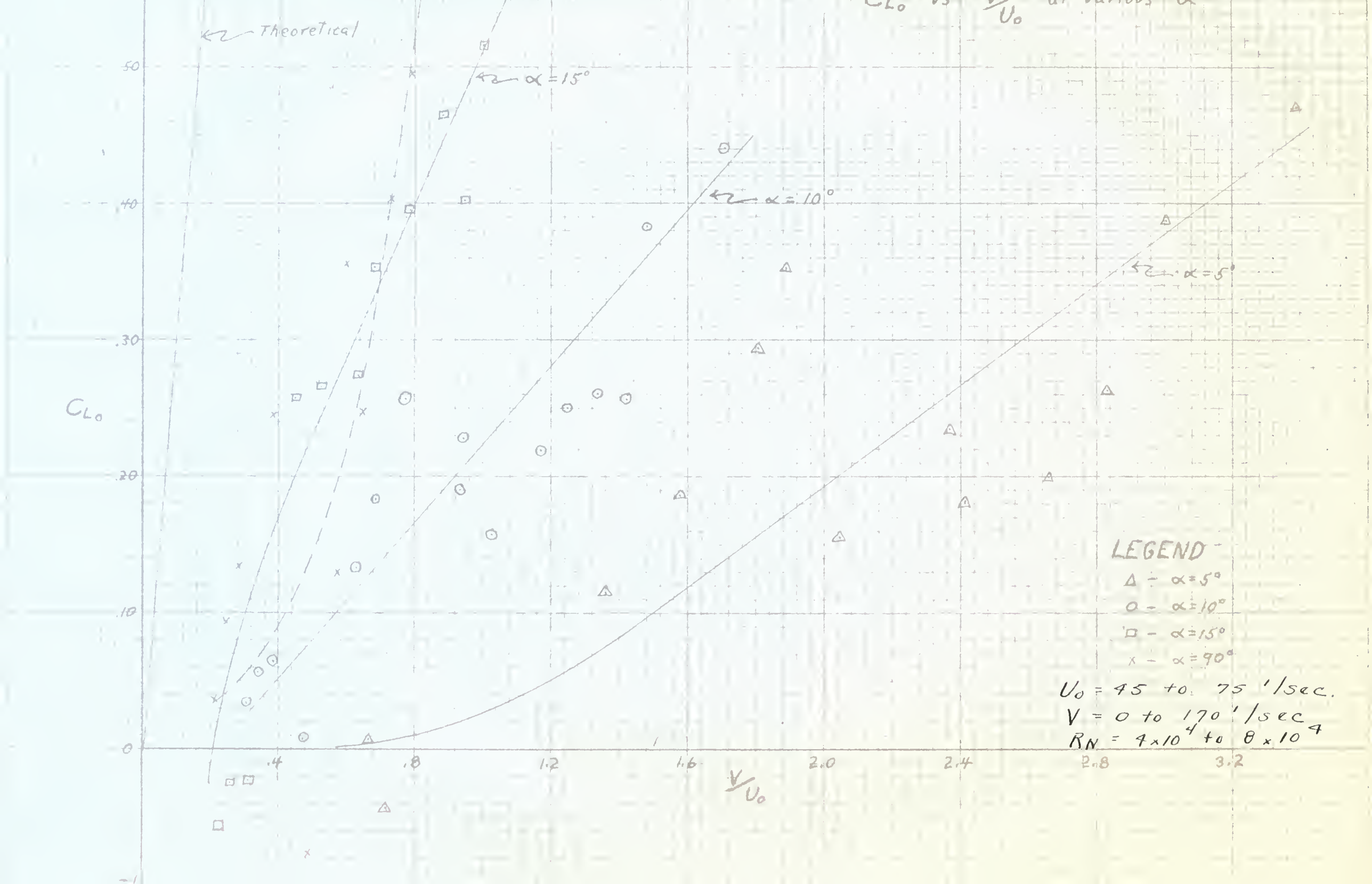

is apparent that at angles of attack greater than 15°, values are obtained which have a resemblance to the theoretically expected values and which agree reasonably well with the data of Betz in Figure IV. However, as the angle of attack is decreased, the Magnus force is decreased for a given V/U_0. There is no ready explanation for this occurrence. Possibly, at the lower angles of attack the flow tends to align itself with the cylinder axis so that the effective cross-flow is less than the cross-flow component of the free stream velocity.

The reliability of the experimental techniques employed is verified by a comparison of the curve of Figure XIX and the curve by Betz in Figure IV. The tests of these two curves are similar and the curves indicate practically identical results in the ranges tested.

Figure XVIII presents the Magnus force coefficient as a function of rotational velocity. It shows that the force varies approximately linearly with rotational velocity as expected from theory.

In general, the data gave a wide dispersion of points on the graphs so that the curves can be regarded as indicating general trends and not specific values. The one exception to this is the data for the case where the axis of the model was perpendicular to the air stream or the relative angle of

FIGURE XVIII

C_L vs R.P.M.

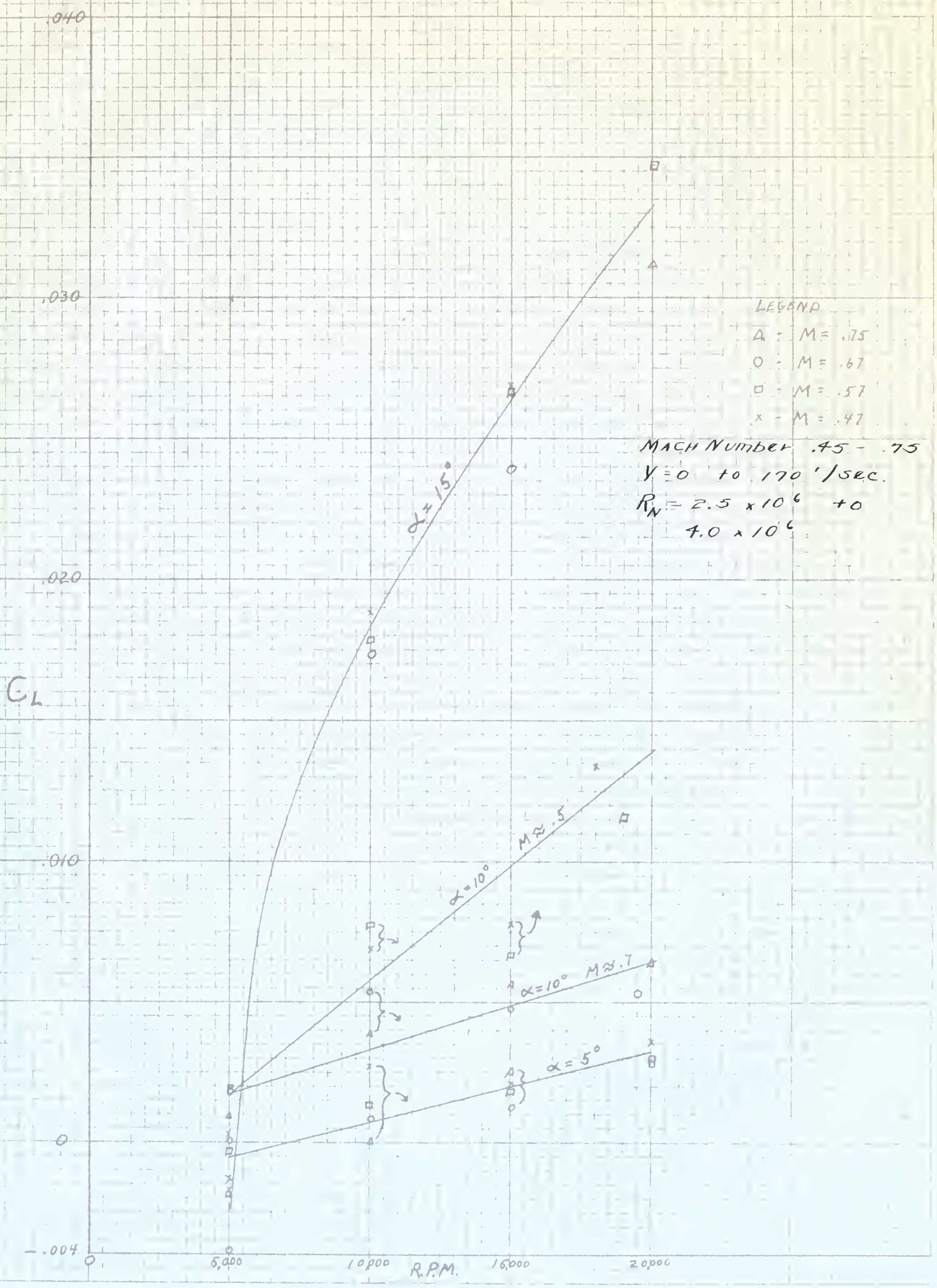

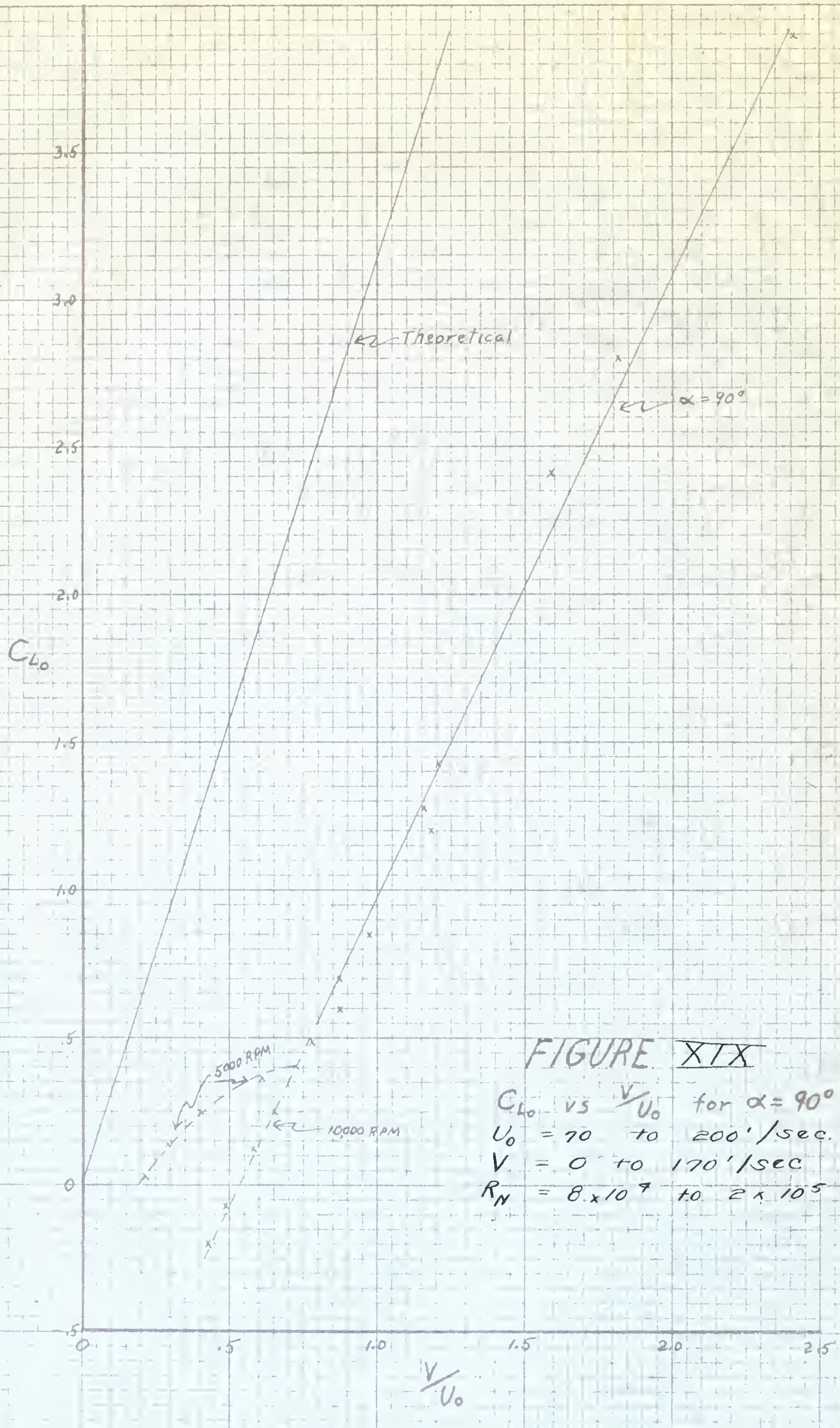

FIGURE XIX

C_{L_0} vs V/U_0 for $\alpha = 90°$

$U_0 = 70$ to $200'/sec.$

$V = 0$ to $170'/sec$

$R_N = 8 \times 10^4$ to 2×10^5

attack was 90°. In this case the data was accurate and consistent, and the curve was drawn through the experimental points.

Data inaccuracy was mainly due to unsteady galvanometer indications. The reliable accuracy for these readings was .3 pound-inches. Every effort was made to reduce this error by careful study of the moments at all strain gage locations. In the test for the 90° angle of attack attitude, low air-speed was used in the wind tunnel with the result that the model did not vibrate and the galvanometer readings were steady and accurate. This indicates the possibility of obtaining more accurate data if the model installation were modified with a view to minimizing or eliminating the vibrations.

As shown on the graphs of Figures XVI and XIX, some negative values for Magnus force were obtained in the vicinity of $V/U_o = .4$. On Figure XVI this might be regarded as data inaccuracy, but on Figure XIX for $\alpha = 90°$ where the data appears reliable, appreciable negative values are obtained. Previous investigators reported zero Magnus force below V/U_o ratios of .5, but it is not known if their appartus was capable of measuring negative forces.

The data for $\alpha = 90°$ of Figure XIX which appears accurate gives another result which is inconsistent with theory, and that is the double curve which occurs below $V/U_o = .7$. The

forces involved were within the accuracy of the equipment for this particular test. Further investigation is necessary to explain this apparent inconsistency.

The center of pressure as obtained from the experiment appeared to be a function of rotational velocity and angle of attack. The effect of free stream velocity on the center of pressure location appeared to be small. The variation in the center of pressure location is presented graphically in Figure XX. In general it appears that at small angles of attack and at the higher rotational velocities where circulation is well developed, the center of pressure shifts forward with decreased angles of attack, indicating that the flow tends to align itself with the cylinder at small angles of attack thus decreasing the effective crossflow component near the downstream end.

In order to find any flow irregularities which might exist, the shadowgraph of Figure XXI was made. It shows that axially sonic velocities were developed on the upstream side of the model, while separation of flow occurs at the angle on the downstream side of the model. No distortion of flow due to rotation is visible. It does not appear that these occurrences had any effect on the Magnus force.

Several factors which may have had an influence on the accuracy of the experimental results, but were not evaluated, will now be mentioned.

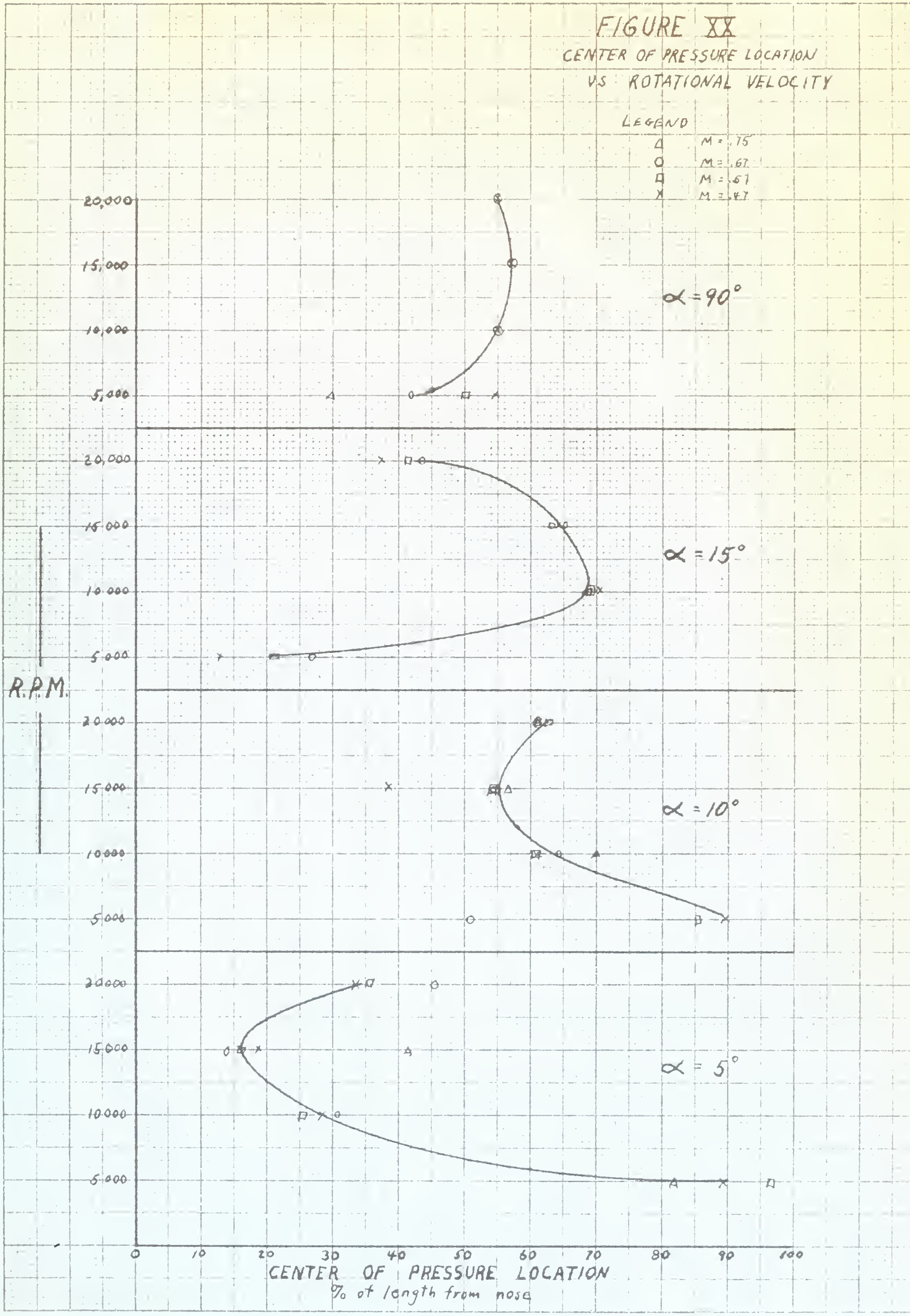
FIGURE XX
CENTER OF PRESSURE LOCATION
VS ROTATIONAL VELOCITY
LEGEND
Δ M = .75
O M = .67
□ M = .57
X M = .47
α = 90°
α = 15°
α = 10°
α = 5°
R.P.M.
20,000
15,000
10,000
5,000
0
10
20
30
40
50
60
70
80
90
100
CENTER OF PRESSURE LOCATION
% of length from nose

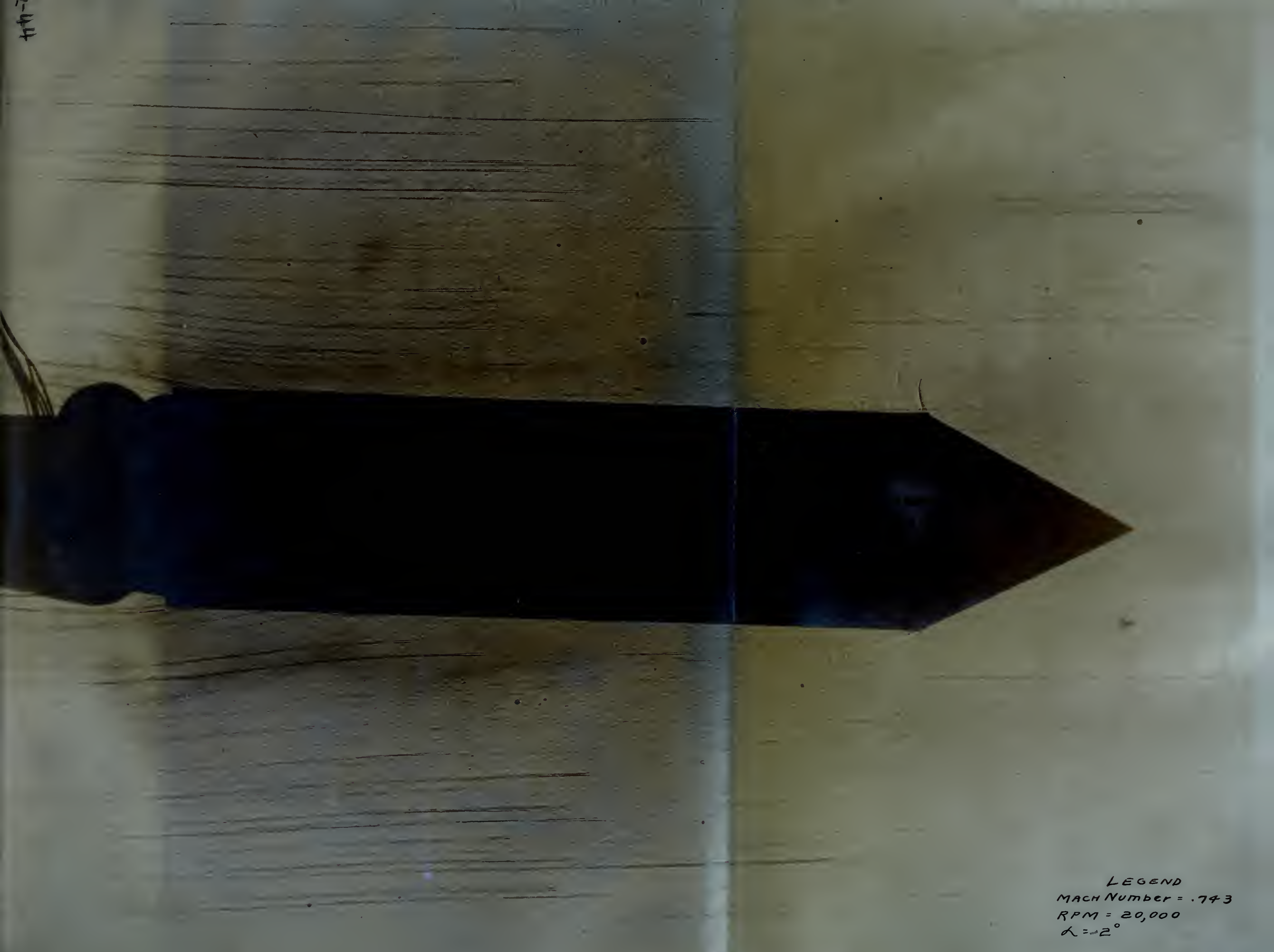

FIG. XX - SHADOWGRAPH OF MODEL DURING TYPICAL RUN

The vibration of the model which was caused by high speed axially incident velocities produced unsteady galvanometer indications which limited the accuracy of readings. The vibration of the model induced by its own rotation was at a high frequency and did not affect the galvanometer readings. However, such vibrations might possibly have some effect on the aerodynamic performance of the model.

The model support blocked some of the endwise flow over the base of the model, thus decreasing the end loss so that the model gave a higher Magnus force than it would give in free flight.

No attempt was made to correct for tunnel wall effect. Experience in the tunnel with other models indicates that this effect is small. Another possible interference effect might have occurred from the model supporting arms; however, the model was far enough from the arms so that the effect would be negligible.

In the test at angle of attack 90°, the base of the model was about 1/16 inch from the tunnel wall. This proximity of the wall eliminated end losses due to spillage and introduced another error due to the tunnel wall boundary layer which, with its lower velocities, would decrease Magnus force, and to some extent compensate for the elimination of end losses. The fact that the experimental and theoretical center of pressure location for this case agreed closely indicates that

the effect of these errors cancelled each other.

III. CONCLUSIONS

1. The Magnus force for a body similar to the one tested may be computed by means of the curve of Figure XVI.

2. The Magnus force for cylindrically shaped bodies at small angles of attack cannot be determined by simplified theoretical computations.

3. At V/U_o ratios below .5, some negative values of Magnus force are obtained. This is entirely inconsistent with theory but is, apparently, a reliable result.

4. The center of pressure location is a function of rotational velocity and angle of attack, and is not sensitive to free stream velocity changes.

5. At angles of attack less than 15° the flow tends to align itself with the axis of the model, thus decreasing the effective crossflow component near the downstream end of the model.

IV. RECOMMENDATIONS

Several possibilities for further investigations are suggested.

1. A modification of the design of the apparatus with a view to the elimination of the low frequency vibrations, or elimination of their effect on galvanometer

indications.

2. Tests of shapes similar to actual missile designs. A more stable nose configuration might also eliminate the low frequency vibration.

3. A thorough investigation of the force in the V/V_o ratio range below .3 where inconsistent results were obtained.

4. A theoretical analysis of the problem as a three-dimensional, compressible, viscous fluid flow problem.

5. Tests of the effect of changing the roughness of the rotating surface.

6. An investigation of the velocity and pressure gradients through the boundary layer around the model.

7. Measurement of the actual pressure existing at the surface of the cylinder while it is rotating.

8. Tests at supersonic velocities approximating the flight of actual missiles.

9. Tests of a cylinder with its axis perpendicular to the air flow at high subsonic velocities.

REFERENCES

1. Magnus; Abhandlungen d. Berliner Akad., 1852.

2. Prandtl, L; Tietjens, O. G., Applied Hydro- and Aero-Dynamics, McGraw-Hill, New York & London, 1934, p. 176, 185.

3. Goldstein, S., Fluid Dynamics, Vol. I and II, Oxford, 1938, p. 546, 33, 81.

4. Prandtl, L., Betz, A., Ergebnisse der Aerodynamischen Versuchsanstalt zu Gottingen, IV, Munchen and Berlin, 1932; "Messungen an rotierenden Zylindern" by Von A. Busemann, P. 101.

5. Millikan, Clark B., Aerodynamics of the Airplane, Wiley & Sons. New York, 1941, p. 39, 40.

6. Sauer, Robert, Introduction to Theoretical Gas Dynamics, J. Edwards, 1947, p. 42.